Three-flavor solar neutrino oscillations with terrestrial neutrino constraints

G.L. Fogli,[1] G. Lettera,[1] E. Lisi,[1] A. Marrone,[1] A. Palazzo,[1] and A. Rotunno[1]

[1] *Dipartimento di Fisica and Sezione INFN di Bari*
Via Amendola 173, 70126 Bari, Italy

Abstract

We present an updated analysis of the current solar neutrino data in terms of three-flavor oscillations, including the additional constraints coming from terrestrial neutrino oscillation searches at the CHOOZ (reactor), Super-Kamiokande (atmospheric), and KEK-to-Kamioka (accelerator) experiments. The best fit is reached for the subcase of two-family mixing, and the additional admixture with the third neutrino is severely limited. We discuss the relevant features of the globally allowed regions in the oscillation parameter space, as well as their impact on the amplitude of possible CP-violation effects at future accelerator experiments and on the reconstruction accuracy of the mass-mixing oscillation parameters at the KamLAND reactor experiment.

PACS numbers: 26.65.+t, 13.15.+g, 14.60.Pq, 91.35.-x

arXiv:hep-ph/0208026 v1 2 Aug 2002

I. INTRODUCTION

In this paper we present an updated three-flavor oscillation analysis of the solar neutrino data coming from the Homestake [1], SAGE [2], GALLEX/GNO [3, 4], Super-Kamiokande (SK) [5], and Sudbury Neutrino Observatory (SNO) [6, 7] experiments. We include additional constraints coming from terrestrial neutrino oscillation searches performed at the CHOOZ reactors [8], at the SK atmospheric ν experiment [9], and at the KEK-to-Kamioka (K2K) long baseline accelerator experiment [10]. Implications for upcoming or future experiments are also discussed. This work extends a previous solar 2ν analysis [11], to which we refer the reader for technical details.

The plan of our paper is as follows. In Sec. II and III we briefly review the theoretical and experimental input, respectively. In Sec. IV we present the results of our 3ν oscillation analysis. In Sec. V we discuss some implications for CP violation searches at future accelerator experiments. In Sec. VI we analyze the accuracy of parameter reconstruction in the Kamioka Liquid scintillator Anti Neutrino Detector (KamLAND) experiment at reactors [12]. We draw our conclusions in Sec. VII.

II. THEORETICAL 3ν FRAMEWORK AND APPROXIMATIONS

We consider standard 3ν oscillations among flavor eigenstates $\nu_\alpha = (\nu_e, \nu_\mu, \nu_\tau)$ and mass eigenstates $\nu_i = (\nu_1, \nu_2, \nu_3)$ with a squared ν mass spectrum defined as

$$(m_1^2,\, m_2^2,\, m_3^2) = \left(-\frac{\delta m^2}{2},\, +\frac{\delta m^2}{2},\, \pm\Delta m^2\right) \,, \tag{1}$$

up to an irrelevant overall constant. The two squared mass gaps δm^2 and Δm^2 (both > 0) are usually referred to as "solar" and "atmospheric" squared mass gaps, respectively. The cases $+\Delta m^2$ and $-\Delta m^2$ identify the so-called direct and inverted spectrum hierarchies [13].[1]

The mixing matrix $U_{\alpha i}$ is parametrized according to the usual convention [14] as

$$U = U(\theta_{12}, \theta_{13}, \theta_{23}) \,, \tag{2}$$

where we have dropped the (currently unobservable) CP violation phase. The mixing angles span two octants, $\theta_{ij} \in [0, \pi/2]$, and are often parametrized in terms of either $\tan^2\theta_{ij}$ (in logarithmic scale) or $\sin^2\theta_{ij}$ (in linear scale) [15, 16]. We use the latter representation in this work.[2]

As it is well known, solar and terrestrial neutrino data consistently favor the so-called hierarchical hypothesis

$$\delta m^2 \ll \Delta m^2 \,, \tag{3}$$

which can be used to simplify the calculations [17]. Even if some regions of the explored parameter space do not fulfill the above hypothesis, the *a posteriori* likelihood of combined

[1] We assume direct hierarchy, unless otherwise stated. As discussed later, the case of inverse hierarchy does not appreciably change the results of our analysis.

[2] The alternative representation in terms of $\log\tan^2\theta_{ij}$ is more useful when the allowed regions span several decades in mixing angles—a situation no longer realized in the current neutrino phenomenology.

solutions in such regions appears to be so low that, at present, the zeroth-order approximation (one-mass-scale dominance [15, 16, 17]) is practically justified in the current analysis of both solar and atmospheric neutrino data.

In particular, solar neutrino oscillations are described with very good accuracy in terms of the 3ν parameter subset $(\delta m^2, \theta_{12}, \theta_{13})$ [16, 18, 19]. Corrections due to violations of Eq. (3) have been shown to be typically small (see [13] and references therein), and can be safely neglected at present. Therefore, in the statistical analysis of the solar ν data, the χ^2 function takes the form:

$$\chi^2_{\rm solar} = \chi^2(\delta m^2, \theta_{12}, \theta_{13}) \ , \tag{4}$$

with no dependence on Δm^2 and thus on the mass spectrum hierarchy (direct or inverse).

Concerning atmospheric neutrinos, it has been shown in several analyses that the usual bounds on the dominant $\nu_\mu \to \nu_\tau$ oscillation parameters $(\Delta m^2, \theta_{23})$ are rather robust under perturbations beyond the one-mass-scale dominance, induced by either $\theta_{13} > 0$ [9, 20, 21, 22] or by $\delta m^2 > 0$ or both [19, 23, 24, 25, 26] (within reactor bounds).[3]

Moreover, since the θ_{23} value is irrelevant for the analysis of both solar and reactor neutrino data, we only need to know the atmospheric Δm^2 scale in our analysis, as derived by a combination of the (preliminary) SK and K2K bounds [9, 10] for unconstrained θ_{23} (see the next section). Summarizing, we use the SK (atmospheric) and K2K bounds to derive the marginal likelihood for Δm^2, namely,

$$\chi^2_{\rm SK+K2K} = \chi^2_{\rm SK+K2K}(\Delta m^2) \ . \tag{5}$$

Such likelihood is practically independent of all the other 3ν parameters (and on the $\pm\Delta m^2$ cases), as far as the hierarchical hypothesis holds phenomenologically.

In the analysis of the CHOOZ reactor constraints, however, the hierarchical approximation may not be accurate enough, and the full 3ν oscillation probability (as reported, e.g., in [13]) must be used in global analyses [21, 25, 28, 29, 30, 31], providing a χ^2 functional dependence of the kind

$$\chi^2_{\rm CHOOZ} = \chi^2_{\rm CHOOZ}(\delta m^2, \pm\Delta m^2, \theta_{12}, \theta_{13}) \ . \tag{6}$$

The reason is that the CHOOZ bounds on $\overline{\nu}_e$ disappearance can be saturated by taking either $\theta_{13} > 0$ or $\delta m^2 > 0$ or both [25, 26, 29, 32], thus providing an anticorrelation between the CHOOZ upper limits on δm^2 and θ_{13} that must be properly taken into account. In other words, the higher δm^2, the lower θ_{13}, in both cases of normal and inverted hierarchy [25, 29]. We will discuss some consequences of such anticorrelation in Sec. V.

Before performing the final combination of SK+K2K+CHOOZ with solar neutrinos, it is useful to project away the functional dependence of the likelihood on Δm^2 by defining a "terrestrial" χ^2 as

$$\chi^2_{\rm terr}(\delta m^2, \theta_{12}, \theta_{13}) = \min_{\Delta m^2} \left(\chi^2_{\rm SK+K2K} + \chi^2_{\rm CHOOZ} \right) \ , \tag{7}$$

which contains only a residual dependence on the hierarchy (direct or inverse) through $\chi^2_{\rm CHOOZ}$. Therefore, in principle, the global combination

$$\chi^2_{\rm global}(\delta m^2, \theta_{12}, \theta_{13}) = \chi^2_{\rm solar} + \chi^2_{\rm terr} \tag{8}$$

also depends on the hierarchy, although, unfortunately, in a very weak way at present.

[3] Moreover, the estimates of the leading parameters $(\Delta m^2, \theta_{23})$ are robust under perturbations induced by new neutrino states or interactions, see [27] and references therein.

III. EXPERIMENTAL INPUT

In this section we briefly review the experimental input coming from solar and terrestrial (atmospheric, reactor, and accelerator) experiments.

For the solar neutrino analysis we use the same standard solar model input and neutrino data (81 observables) as in [11], but with an updated winter-summer rate difference from the combination of GALLEX/GNO [4][4] and SAGE [2] measurements,

$$R_W - R_S \simeq -5 \pm 7 \text{ SNU} \quad (\text{GALLEX/GNO} + \text{SAGE}) \, . \tag{9}$$

Concerning reactor data, we take the CHOOZ absolute spectrum from [8]. The 3ν analysis includes the 7+7 bin spectra as in [13].

Concerning atmospheric neutrinos, the SK collaboration has recently presented updated (92 kton yr) bounds on the leading $\nu_\mu \to \nu_\tau$ atmospheric neutrino oscillation parameters $(\Delta m^2, \sin^2 2\theta_{23})$ [9]. Since the correlation between the two parameters appears to be negligible, the bounds on Δm^2 for unconstrained (i.e., projected) values of $\sin^2 2\theta_{23}$ are basically obtained by fixing $\sin^2 2\theta_{23}$ at its the best fit value (unity). From a graphical reduction of the bounds shown in [9], we derive then an approximate $\Delta\chi^2_{\rm SK}$ function in terms of Δm^2.

The K2K Collaboration has also presented preliminary bounds on the same mass-mixing parameters $(\Delta m^2, \sin^2 2\theta_{23})$ [10], again with apparently negligible correlation around the best fit point (as far as $\sin^2 2\theta_{23}$ is nearly maximal). The bounds on $\sin^2 2\theta_{23}$ are relatively weak, but those on Δm^2 are already competitive with those placed by SK and must be taken into account. We simply do so by a graphical reduction of the $\Delta\chi^2_{\rm K2K}$ function presented in [10] for maximal mixing, to be combined (summed) with the previous $\Delta\chi^2_{\rm SK}$.

It turns out that the function $\Delta\chi^2_{\rm SK+K2K}$ obtained in this way is nearly parabolic in the *linear* variable Δm^2, although the separate $\Delta\chi^2_{\rm SK}$ and $\Delta\chi^2_{\rm K2K}$ components are not parabolic. The SK+K2K χ^2 minimum is at 2.7×10^{-3} eV^2, with a $\pm 1\sigma$ error ($\Delta\chi^2_{\rm SK+K2K} = 1$ for $N_{\rm DF} = 1$) equal to $\sim 0.4 \times 10^{-3}$ eV^2. The estimated range for Δm^2, as discussed in the previous section, is known to be very stable under small perturbations induced by nonzero values of θ_{13} or δm^2. Therefore, we use the following SK+K2K combination,

$$\Delta m^2 \simeq (2.7 \pm 0.4) \times 10^{-3} \text{ eV}^2 \tag{10}$$

with approximately linear, symmetrical and gaussian errors, for unconstrained values of the other 3ν parameters. Notice that values of Δm^2 below 1.5×10^{-3} eV^2 are excluded at 3σ, corroborating the trend of a previous SK+K2K combination [33], and reinforcing the validity of Eq. (3). Of course, it will be desirable to confirm this nice result by undertaking a thorough and *ab initio* analysis and combination of the K2K and SK data. We plan to do so when such preliminary data will be published and described in more detail.[5]

IV. RESULTS

In this section we describe the main results of our 3ν solar neutrino oscillation analysis with additional terrestrial constraints. We start from the subcase of 2ν oscillations.

---

[4] Corrected to remove eccentricity effects.

[5] In particular, the K2K *spectral shape* analysis leading to the results in [10] appears to involve much more (and currently unpublished) information than it was required in the simpler analysis of the *total rate* only [33].

TABLE I: Absolute and local best fits for the 2ν analysis reported in Fig. 1 (without CHOOZ). The value $\chi^2_{\rm min} = 72.3$, reached in the LMA solution, corresponds to a good overall fit to 81 solar neutrino data (minus 2 free parameters).

Solution	δm^2 (eV^2)	$\sin^2\theta_{12}$	$\Delta\chi^2$
LMA	5.5×10^{-5}	0.30	–
QVO	6.5×10^{-10}	0.55	7.5
LOW	7.3×10^{-8}	0.41	10.5

A. 2ν oscillations

In the subcase of pure 2ν oscillations ($\theta_{13} = 0$), the information on Δm^2 coming from SK+K2K is completely decoupled within our approximations, and the solar+CHOOZ ν parameter space reduces to $(\delta m^2, \theta_{12})$.

Figure 1 shows the constraints coming from the global solar neutrino analysis in the $(\delta m^2, \sin^2\theta_{12})$ plane, with and without CHOOZ. In the case of solar ν data only, the solutions are almost coincident with those presented in Fig. 1 of [11], modulo the small changes induced by the updated input from Eq. (9) and by the different abscissa. For completeness, Table I gives the local χ^2 minima for the so-called large mixing angle (LMA), quasivacuum oscillation (QVO) and low-δm^2 (LOW) solutions. These minima are not altered by the inclusion of the CHOOZ data, whose only effect is to slightly strengthen the upper bounds on δm^2, as shown in Figure 1. The features of such 2ν allowed regions have been discussed in a number of papers [5, 7, 34, 35, 36, 37, 38, 39] and are not repeated here.

B. 3ν oscillations

Figure 2 shows sections of the volume allowed by solar neutrino data only in the 3ν parameter space $(\delta m^2, \sin^2\theta_{12}, \sin^2\theta_{13})$, for four representative values of $\sin^2\theta_{13}$ (equal to 0, 0.02, 0.04, and 0.06). The best fit is reached in the same LMA point as for the 2ν case ($\sin^2\theta_{13} = 0$). The constraints are derived through Eq. (4) and $N_{\rm DF} = 3$. It can be seen that, for increasing $\sin^2\theta_{13}$, the upper bounds on δm^2 in the LMA become slightly weaker, and the LOW and QVO solutions become less unlikely. Maximal (ν_1, ν_2) mixing ($\sin^2\theta_{12} = 1/2$) is also less disfavored for increasing $\sin^2\theta_{13}$. This trend is qualitatively consistent with the recent results in [38] (obtained for an almost equivalent solar ν data set), as well as with previous 3ν analyses of solar neutrino data [18, 21, 31, 40].

Looser constraints on either δm^2 or maximal mixing can be a desirable property from a theoretical or experimental point of view. Relatively large values of δm^2 are, e.g., required for the possible detection of leptonic CP violation in future (very) long baseline experiments (see, e.g., [41]). Nearly maximal mixing can allow certain cancellations in $0\nu2\beta$ decay or in ν model building (see, e.g., [42]). Unfortunately, such "desirable" features in Fig. 2 are severely limited by the inclusion of current terrestrial data through Eqs. (7) and (8). This is shown in Fig. 3, where the addition of the terrestrial ν constraints actually strengthens the upper bounds on δm^2 for increasing $\sin^2\theta_{13}$, since the CHOOZ bounds are more quickly saturated. Notice also that, in comparison with earlier analyses, the current K2K+SK bounds on Δm^2 [Eq. (10)] are now sufficiently strong to prevent the occurrence of relatively low values of

Δm^2 ($\lesssim 1.5 \times 10^{-3}$ eV^2), where the CHOOZ bounds would become significantly weaker. Therefore, the current SK+K2K data enhance the impact of terrestrial constraints on the solar 3ν parameters $(\delta m^2, \sin^2\theta_{12}, \sin^2\theta_{13})$.

Figure 4 provides another way of looking at the results of the solar+terrestrial analysis. In this figure, the $\Delta\chi^2$ function is projected onto one parameter at a time, so that the n-sigma bounds on each of them (the others being unconstrained) are simply given by a $\Delta\chi^2 = n^2$ cut. In the left panel it can be seen that the χ^2 difference between the LMA and the LOW or QVO solutions is slightly lowered in the 3ν fit, as compared with the 2ν case reported in Table I. However, such improvement for the LOW and QVO solutions for nonzero θ_{13} is currently marginal (less than one unit in $\Delta\chi^2$). Basically all data converge towards zero or low values of $\sin^2\theta_{13}$, whose global upper bounds are reported in the right panel of Fig. 4. In particular, one gets

$$\sin^2\theta_{13} < 0.05 \ (3\sigma, \ N_{\rm DF} = 1) \ , \tag{11}$$

for unconstrained values of the other 3ν parameters.

In conclusion, genuine 3ν mixing in solar neutrinos is severely constrained by terrestrial data. For the most favored solution, increasing θ_{13} corresponds to lowering the upper bound on δm^2. For the less favored LOW and QVO solutions, the improvement of the fit for slightly nonzero values of θ_{13} (see also [38]) is not statistically significant. Figures 3 and 4 quantify such effects.

A final remark is in order. Figures 3 and 4 refer to the case of direct neutrino spectrum hierarchy. We have verified that the changes for inverse hierarchy (not shown) are negligible. Indeed, the phenomenological difference between the two hierarchies, which vanishes for $\theta_{13} \to 0$, is still too small to emerge for the nonzero values of θ_{13} allowed by Eq. (11).

V. IMPLICATIONS FOR FUTURE CP VIOLATION SEARCHES

The anticorrelation between the upper bounds on δm^2 and $\sin^2\theta_{13}$ shown in Fig. 3 is not a particularly desirable feature for future CP violation searches at accelerators, where the difference between the ν and $\overline{\nu}$ oscillation probabilities would be enhanced for *both* δm^2 and θ_{13} close to their upper limits (see, e.g., the reviews in [41]).

In order to study in more detail the maximum CP violation effects compatible with current bounds, we think it useful to focus on the following benchmark quantity, which typically appears as an overall prefactor modulating CP-violating amplitudes, and which has the useful property to be a vacuum-matter (VM) invariant [43]:

$$\begin{aligned} I_{\rm VM} &= (m_1^2 - m_2^2)(m_2^2 - m_3^2)(m_3^2 - m_1^2) \sin 2\theta_{12} \sin 2\theta_{13} \cos\theta_{13} & (12) \\ &= \delta m^2 \left[4(\Delta m^2)^2 - (\delta m^2)^2\right] \sin\theta_{12} \cos\theta_{12} \sin\theta_{13} \cos^2\theta_{13} \ . & (13) \end{aligned}$$

More precisely, in order to eliminate the dependence on Δm^2 and to simplify the discussion, we integrate $I_{\rm VM}$ over the gaussian distribution in Δm^2 defined in Eq. (10), obtaining the expectation value

$$\overline{I}_{\rm VM} = \delta m^2 \left[4(\Delta m_0^2)^2 + 4(\sigma_\Delta)^2 - (\delta m^2)^2\right] \sin\theta_{12} \cos\theta_{12} \sin\theta_{13} \cos^2\theta_{13} \ , \tag{14}$$

where $\Delta m_0^2 = 2.7 \times 10^{-3}$ eV^2 and $\sigma_\Delta = 0.4 \times 10^{-3}$ eV^2 [Eq. (10)]. The quantity $\overline{I}_{\rm VM}$ is then a function of the same 3ν parameters $(\delta m^2, \theta_{12}, \theta_{13})$ used for the previous solar+terrestrial

analysis. Notice that $\overline{I}_{\rm VM} \to 0$ when any of these 3ν parameters tends to zero, as intuitively expected for a quantity associated to CP violation [43].

Figure 5 shows isolines of $\overline{I}_{\rm VM}$ in the plane $(\delta m^2, \sin^2\theta_{12})$, for the same representative values of $\sin^2\theta_{13}$ as in Figs. 2 and 3. The δm^2 scale is restricted to the range relevant for the LMA solution, whose C.L. contours are superposed in each panel (as taken from Fig. 3). In the upper left panel ($\sin^2\theta_{13} = 0$), the vacuum-matter invariant $\overline{I}_{\rm VM}$ is identically zero. In other panels, it can be seen that $\overline{I}_{\rm VM}$ achieves its maximum values, within the LMA solution, for "intermediate" values of $\sin^2\theta_{13}$ ($\simeq 0.02$–0.04). Indeed, for increasing values of $\sin^2\theta_{13}$ the LMA upper bound on δm^2 decreases, and $\overline{I}_{\rm VM}$ is maximized when a compromise is reached. We conclude that the maximum allowed amplitude of possible CP violation effects (in future accelerator experiments) occurs somewhat below the upper bound placed by terrestrial experiments on $\sin^2\theta_{13}$, due to the phenomenological anticorrelation with the δm^2 upper bound.

VI. IMPLICATIONS FOR KAMLAND

The KamLAND experiment is currently detecting reactor $\overline{\nu}_e$ events, whose energy spectrum will provide soon a clear terrestrial test of the solar ν LMA solution [12]. If the LMA solution is disconfirmed, the BOREXINO experiment will be able to test the remaining LOW and QVO solutions by detecting time variations of the event rate [44]. Assuming that the LMA solution is confirmed, various studies have shown how well the KamLAND experiment can reconstruct the oscillation parameters for a few selected points in the $(\delta m^2, \theta_{12})$ parameter space [12, 45, 46, 47, 48, 49, 50, 51]. In this section we extend these studies by performing a continuous scan in the δm^2 parameter, in the region of interest for the LMA solution.

In the analysis, we use standard inputs for the reactor average fuel composition [52], $\overline{\nu}_e$ energy spectra [53] and cross section [54]. We take from [55] the reactor power and locations. The visible energy window is chosen to be $E \in [1.22, 7.22]$ MeV (divided in 12 bins) as in [48, 49], with energy resolution $\sigma(E)/\sqrt{E} = 5\%$ (E in MeV) [12]. We assume a "KamLAND year" corresponding to 550 events/yr for no oscillation [12], and consider two representative exposure periods of 0.5 and 3 years, the shortest period being a tentative estimate of the detector live-time that might be used for the first official release of the KamLAND data.

Concerning the uncertainties, in addition to the statistical fluctuations in each bin, we include a $\sim 4\%$ overall normalization error [12] (due to uncertainties in fiducial volume, ν flux, and cross section), and a 2% energy scale uncertainty [12]. The normalization and energy scale systematics (fully correlated in each bin) mainly worsen the reconstruction accuracy of $\sin^2\theta_{12}$ and δm^2, respectively. Background reduction and subtraction are still in progress at KamLAND [12], and we do not include the (unknown) associated errors in the analysis. More realistic analyses, including backgrounds and other systematics (e.g., fuel composition uncertainties [45]), will be possible after release of the real KamLAND data and of related information.

Given the above input, for fixed *true* values of the parameters $(\delta m^2, \sin^2\theta_{12})$ we first determine the $\Delta\chi^2 \leq 4$ region including the *reconstructed* oscillation parameters, and then project this region either on δm^2 or on $\sin^2\theta_{12}$, in order to obtain the $\pm 2\sigma$ error bands on each of the two oscillation parameters separately. For simplicity, this procedure is done for fixed $\theta_{13} = 0$. When real KamLAND data will be available, a more complete analysis procedure (not simulated here) should include a variable θ_{13} parameter, to be constrained

by world neutrino data (as previously done for the currently available data in Figs 3 and 4). Small variations of θ_{13} would then basically act as an additional KamLAND normalization uncertainty [49].

Figure 6 shows the $\pm 2\sigma$ range of the reconstructed δm^2, as a function of the true value of δm^2. The true value of $\sin^2\theta_{12}$ is fixed at 0.3 (LMA best-fit), while the reconstructed $\sin^2\theta_{12}$ is projected away. It can be seen that, in the range most relevant for the LMA solution ($\delta m^2 \sim$ few $\times 10^{-5}$ eV^2) the reconstruction accuracy depends only weakly on δm^2. It become rapidly worse, however, outside this range. E.g., for low values of δm^2 (approaching the no-oscillation limit in KamLAND), the reconstructed value of δm^2 can be considerably higher than the true one, the variation being compensated by a lower value of the reconstructed $\sin^2\theta_{12}$. For high values of δm^2 (say, $\gtrsim 10^{-4}$ eV^2), degenerate solutions begin to appear, eventually leading to a tower of (merging) multiple ranges for the reconstructed δm^2. For a half-year exposure, an isolated, low-δm^2 reconstructed range also appears, since the spectrum suppression due to true values $\delta m^2 \gtrsim 10^{-4}$ eV^2 can be confused with a similar suppression induced by lower values of both δm^2 *and* $\sin^2\theta_{12}$. Such ambiguities can be cleared up, e.g., after 3 years of data taking, provided that $\delta m^2 \lesssim 2 \times 10^{-4}$ eV^2. Above this range, KamLAND cannot resolve the pattern of fast oscillations in the $\overline{\nu}_e$ energy spectrum, which could be disentangled only by reducing the typical baseline [30, 50, 56].

Figure 7 zooms in on true δm^2 values below 2×10^{-4} eV^2, for three representative (true) values of $\sin^2\theta_{12}$. For oscillation parameters close to the LMA ones, the accuracy in the δm^2 reconstruction can already be as good as $\sim \pm 10\%$ at 2σ after half-year exposure, and can improve by a factor of ~ 2 after three years. The δm^2 reconstruction accuracy improves (worsens) slightly for increasing (decreasing) values of $\sin^2\theta_{12}$, since this parameter governs the amplitude of the oscillation pattern, from which δm^2 is inferred.

Finally, Fig. 8 shows the reconstructed range of $\sin^2\theta_{12}$ (first octant only), for the same choice of true oscillation parameters as in Fig. 7. From this figure it appears that the most accurate reconstruction of $\sin^2\theta_{12}$ occurs for δm^2 values slightly below the current LMA best-fit point. The reason is that, for such relatively low values, the overall rate suppression in KamLAND is maximized, making it easier to put bounds on the oscillation amplitude and thus on $\sin^2\theta_{12}$. The $\sin^2\theta_{12}$ reconstruction accuracy tends to become constant for high values of δm^2 (regime of fast oscillations). In the lower panel, notice the appearance of a degenerate reconstructed range for the case of 0.5 year exposure, which has the same origin as the corresponding one discussed in Fig. 6.

In conclusion, KamLAND is in an extremely favorable situation to fix the most likely values of δm^2 in the LMA region within a few % error. The achievable accuracy in the $\sin^2\theta_{12}$ reconstruction is instead both lower and more uncertain, and will depend very much on how the real KamLAND data will look like.

VII. CONCLUSIONS

We have studied the 3ν perturbations to the usual 2ν solutions to the solar neutrino problem, including—besides the full set of current solar data—the terrestrial neutrino constraints coming from the CHOOZ (reactor), SK (atmospheric) and K2K (accelerator) experiments. The global best fit is reached in the so-called LMA solution, for the subcase of 2ν mixing ($\theta_{13} = 0$). The likelihood of the (less favored) LOW and QVO solutions does not improve significantly for nonzero θ_{13}, within the severe constraints placed by terrestrial neutrino experiments on such mixing angle. The anticorrelation between the upper bounds on δm^2

and θ_{13} has been discussed, together with its implications for the maximum allowed amplitude of possible CP violation effects (expressed in terms of a representative vacuum-matter invariant). We have also discussed the expected accuracy of the mass-mixing parameter reconstruction in the (currently running) KamLAND experiments, described through a continuous scan of the δm^2 parameter within the LMA solution.

Acknowledgments

E.L. thanks the organizers of the Summer Institute "New Dimensions in Astroparticle Physics" (Gran Sasso National Laboratory, Assergi, Italy, 2002), where preliminary results of this work were presented, for kind hospitality. This work was supported in part by INFN and in part by the Italian *Ministero dell'Istruzione, Università e Ricerca* through the "Astroparticle Physics" research project.

---

[1] Homestake Collaboration, B. T. Cleveland *et al.*, Astrophys. J. **496**, 505 (1998).
[2] SAGE Collaboration, J. N. Abdurashitov *et al.*, astro-ph/0204245 v2.
[3] GALLEX Collaboration, W. Hampel *et al.*, Phys. Lett. B **447**, 127 (1999).
[4] T. Kirsten for the GNO Collaboration, in *Neutrino 2002*, 20th International Conference on Neutrino Physics and Astrophysics (Munich, Germany, 2002). Transparencies available at the URL: neutrino2002.ph.tum.de .
[5] Super-Kamiokande Collaboration, S. Fukuda *et al.*, hep-ex/0205075.
[6] SNO Collaboration, Q. R. Ahmad *et al.*, Phys. Rev. Lett. **89**, 011301 (2002).
[7] SNO Collaboration, Q. R. Ahmad *et al.*, Phys. Rev. Lett. **89**, 011302 (2002).
[8] CHOOZ Collaboration, M. Apollonio *et al.*, Phys. Lett. B **466**, 415 (1999).
[9] M. Shiozawa for the Super-Kamiokande Collaboration, in *Neutrino 2002* [4].
[10] K. Nishikawa for the K2K Collaboration, in *Neutrino 2002* [4].
[11] G. L. Fogli, E. Lisi, A. Marrone, D. Montanino, and A. Palazzo, hep-ph/0206162, to appear in Phys. Rev. D.
[12] J. Shirai for the KamLAND Collaboration, in *Neutrino 2002* [4].
[13] G. L. Fogli, E. Lisi and A. Palazzo, Phys. Rev. D **65**, 073019 (2002).
[14] Particle Data Group, K. Hagiwara *et al.*, Phys. Rev. D **66**, 010001 (2002).
[15] G. L. Fogli, E. Lisi and G. Scioscia, Phys. Rev. D **52**, 5334 (1995); G. L. Fogli, E. Lisi, D. Montanino and G. Scioscia, Phys. Rev. D **55**, 4385 (1997).
[16] G. L. Fogli, E. Lisi and D. Montanino, Phys. Rev. D **54**, 2048 (1996).
[17] G. L. Fogli, E. Lisi and D. Montanino, Phys. Rev. D **49**, 3626 (1994).
[18] G. L. Fogli, E. Lisi, D. Montanino and A. Palazzo, Phys. Rev. D **62**, 013002 (2000).
[19] G. L. Fogli, E. Lisi and D. Montanino, Astropart. Phys. **4**, 177 (1995).
[20] G. L. Fogli, E. Lisi and A. Marrone, Phys. Rev. D **64**, 093005 (2001).
[21] M. C. Gonzalez-Garcia, M. Maltoni, C. Pena-Garay and J. W. Valle, Phys. Rev. D **63**, 033005 (2001).
[22] O. Yasuda, Phys. Rev. D **58**, 091301 (1998).
[23] A. Strumia, JHEP **9904**, 026 (1999).
[24] T. Teshima and T. Sakai, Phys. Rev. D **62**, 113010 (2000).

[25] A. Marrone, in the Proceedings of *Noon 2001*, 3rd International Workshop on Neutrino Oscillations and their Origin (Tokyo, Japan 2001). Transparencies available at the URL: www-sk.icrr.u-tokyo.ac.jp/noon2001 .
[26] M. C. Gonzalez-Garcia and M. Maltoni, hep-ph/0202218.
[27] Gian Luigi Fogli, E. Lisi, A. Marrone, D. Montanino, and A. Palazzo, in the Proceedings of *TAUP 2001*, 7th International Workshop on Topics in Astroparticle and Underground Physics (Assergi, Italy, 2001), Nucl. Phys. B **110** (Proc. Suppl.), 268 (2002).
[28] Gian Luigi Fogli, E. Lisi, A. Marrone, and A. Palazzo, Proceedings of the 36th Rencontres de Moriond on Electroweak Interactions and Unified Theories (Les Arcs, France, 2001), hep-ph/0104221.
[29] S. M. Bilenky, D. Nicolò, and S. T. Petcov, Phys. Lett. B **538**, 77 (2002)
[30] S. T. Petcov and M. Piai, Phys. Lett. B **533**, 94 (2002).
[31] A. Bandyopadhyay, S. Choubey, S. Goswami, and K. Kar, Phys. Rev. D **65**, 073031 (2002).
[32] I. Mocioiu and R. Shrock, JHEP **0111**, 050 (2001).
[33] G. L. Fogli, E. Lisi, and A. Marrone, Phys. Rev. D **65**, 073028 (2002).
[34] V. Barger, D. Marfatia, K. Whisnant, and B. P. Wood, Phys. Lett. B **537**, 179 (2002).
[35] P. Creminelli, G. Signorelli, and A. Strumia, JHEP **0105**, 052 (2001), hep-ph/0102234 v3.
[36] A. Bandyopadhyay, S. Choubey, S. Goswami, and D. P. Roy, Phys. Lett. B **540**, 14 (2002).
[37] J. N. Bahcall, M. C. Gonzalez-Garcia, and C. Pena-Garay, hep-ph/0204314.
[38] P. C. de Holanda and A. Yu. Smirnov, hep-ph/0205241.
[39] A. Strumia, C. Cattadori, N. Ferrari, and F. Vissani, hep-ph/0205261.
[40] M. C. Gonzalez-Garcia and Y. Nir, hep-ph/0202058.
[41] See talks by M. Lindner and by T. Nakaya at *Neutrino 2002* [4].
[42] G. Altarelli and F. Feruglio, to appear in *Neutrino Mass*, Springer Tracts in Modern Physics, ed. by G. Altarelli and K. Winter, hep-ph/0206077.
[43] See K. Kimura, A. Takamura, and H. Yokomakura, hep-ph/0205295, and references therein.
[44] G. Bellini for the BOREXINO Collaboration, in *Neutrino 2002* [4].
[45] H. Murayama and A. Pierce, Phys. Rev. D **65**, 013012 (2002).
[46] V. D. Barger, D. Marfatia and B. P. Wood, Phys. Lett. B **498**, 53 (2001).
[47] R. Barbieri and A. Strumia, JHEP **0012**, 016 (2000).
[48] A. de Gouvea and C. Pena-Garay, Phys. Rev. D **64**, 113011 (2001).
[49] M. C. Gonzalez-Garcia and C. Pena-Garay, Phys. Lett. B **527**, 199 (2002).
[50] A. Strumia and F. Vissani, JHEP **0111**, 048 (2001).
[51] P. Aliani, V. Antonelli, M. Picariello, and E. Torrente-Lujan, hep-ph/0207348.
[52] Y. Declais *et al.*, Nucl. Phys. B **434**, 503 (1995).
[53] P. Vogel and J. Engel, Phys. Rev. D **39**, 3378 (1985).
[54] P. Vogel and J.F. Beacom, Phys. Rev. D **60**, 053003 (1999).
[55] KamLAND Collaboration, J. Busenitz *et al.*, Proposal for U.S. Participation in KamLAND (unpublished).
[56] S. Schönert, T. Lasserre, and L. Oberauer, hep-ex/0203013.

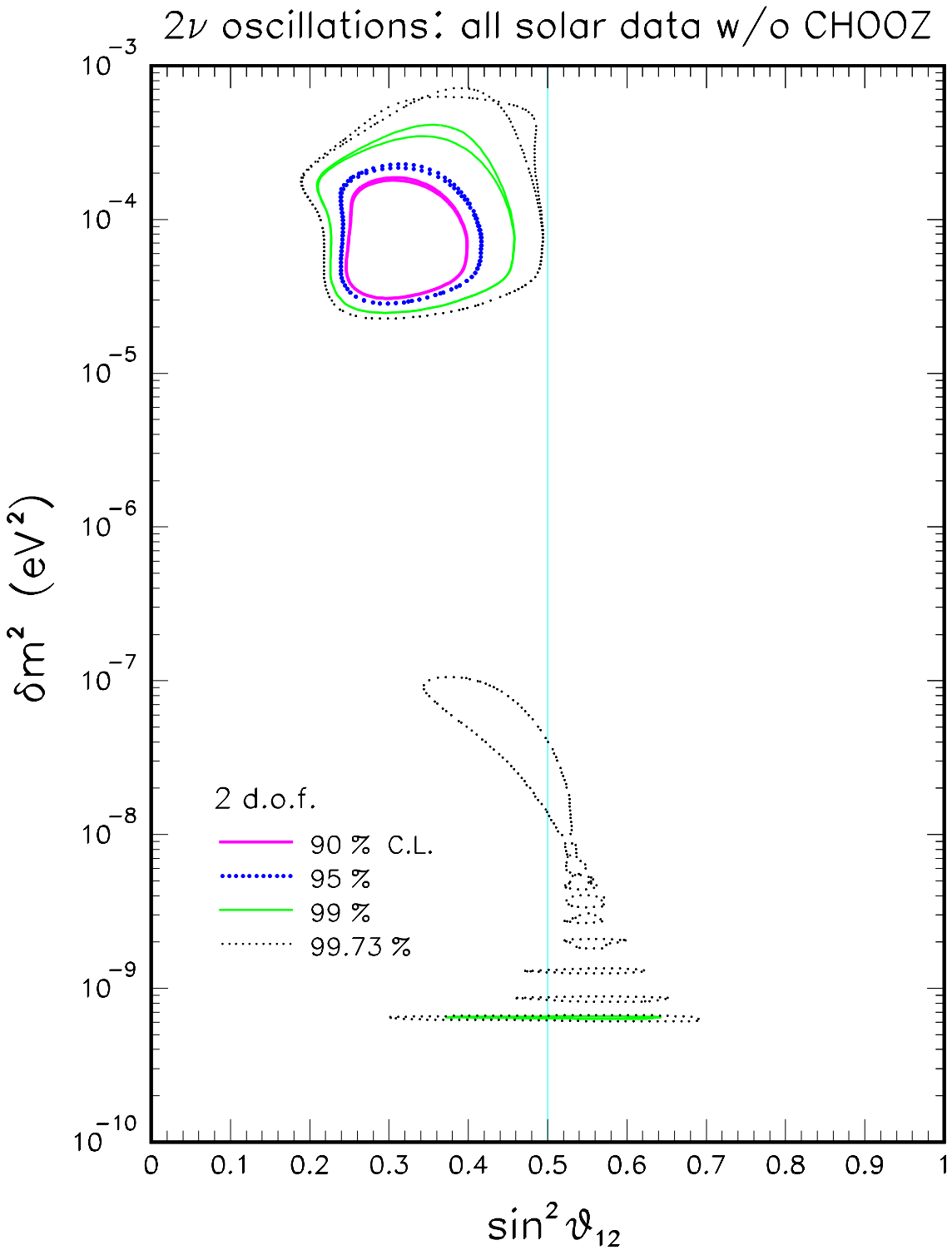

FIG. 1: Two-flavor global analysis of solar neutrino oscillations in the $(\delta m^2, \sin^2\theta_{12})$ parameter space, with and without the additional constraints placed by the CHOOZ reactor experiment. The inclusion of CHOOZ leads to slightly more restrictive upper bounds on δm^2.

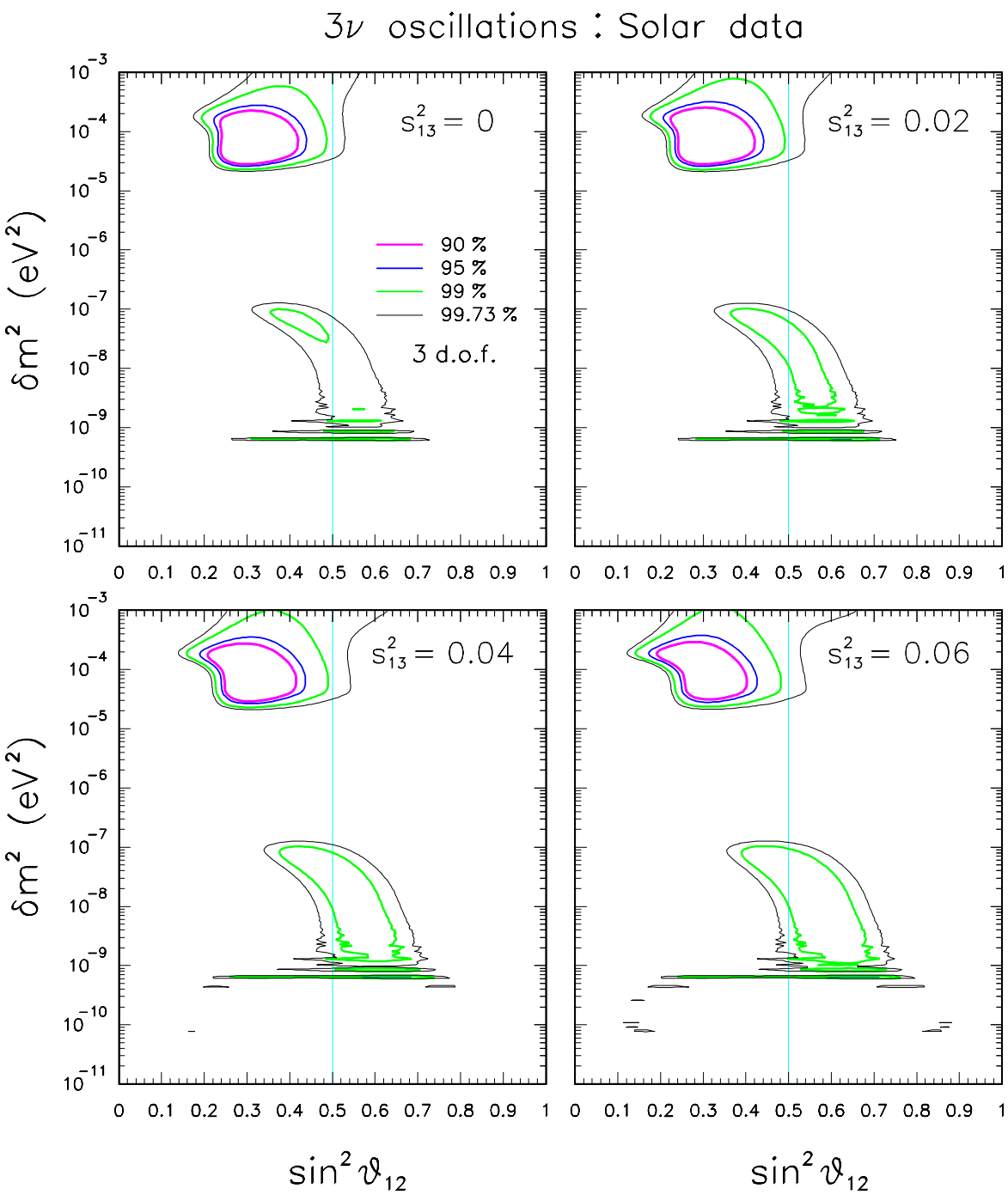

FIG. 2: Three-flavor global analysis of solar neutrino oscillations in the $(\delta m^2, \sin^2\theta_{12}, \sin^2\theta_{13})$ parameter space, shown through four sections at fixed values of $s^2_{13} \equiv \sin^2\theta_{13}$.

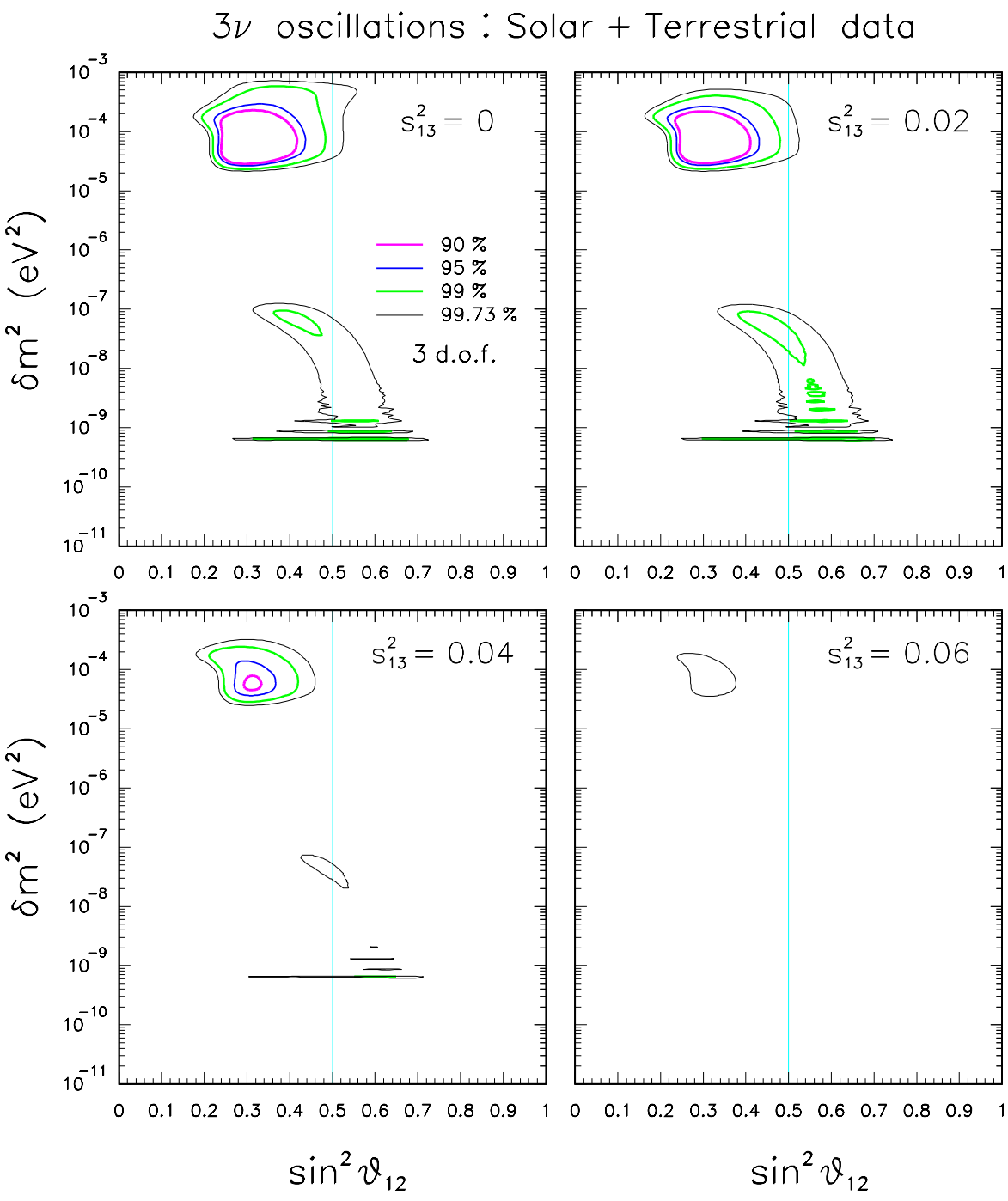

FIG. 3: As in Fig. 2, but including the constraints from terrestrial neutrino oscillation searches at CHOOZ, SK, and K2K.

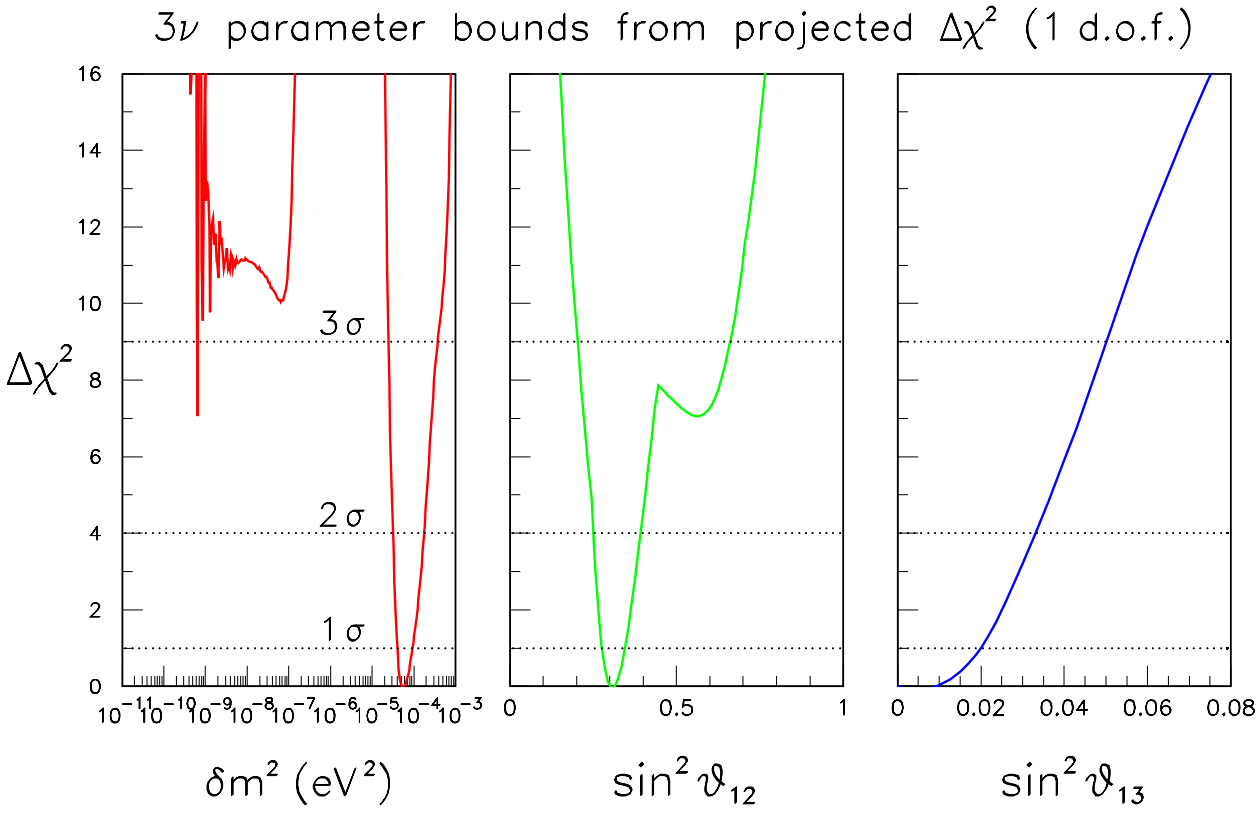

FIG. 4: Projections of the global (solar+terrestrial) $\Delta\chi^2$ function onto each of the $(\delta m^2, \sin^2\theta_{12}, \sin^2\theta_{13})$ parameters. The n-sigma bounds on each parameter (the others being unconstrained) correspond to $\Delta\chi^2 = n^2$.

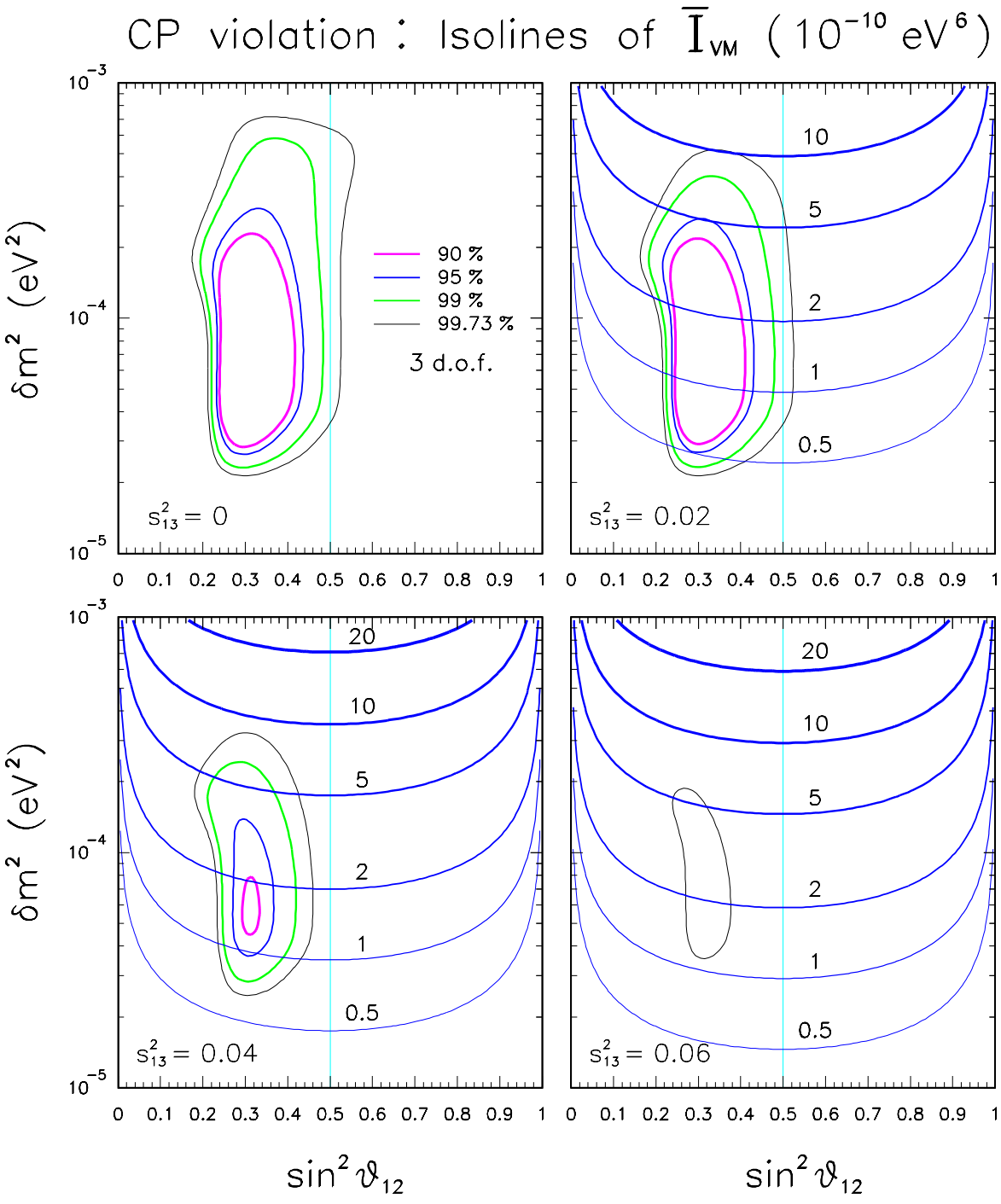

FIG. 5: Isolines of the vacuum-matter invariant $\overline{I}_{\rm VM}$, in units of 10^{-10} eV^6. Superposed are the contours of the large mixing angle solution. The invariant $\overline{I}_{\rm VM}$ appears as a typical prefactor in CP violating amplitudes expected at future accelerator searches; see the text for details.

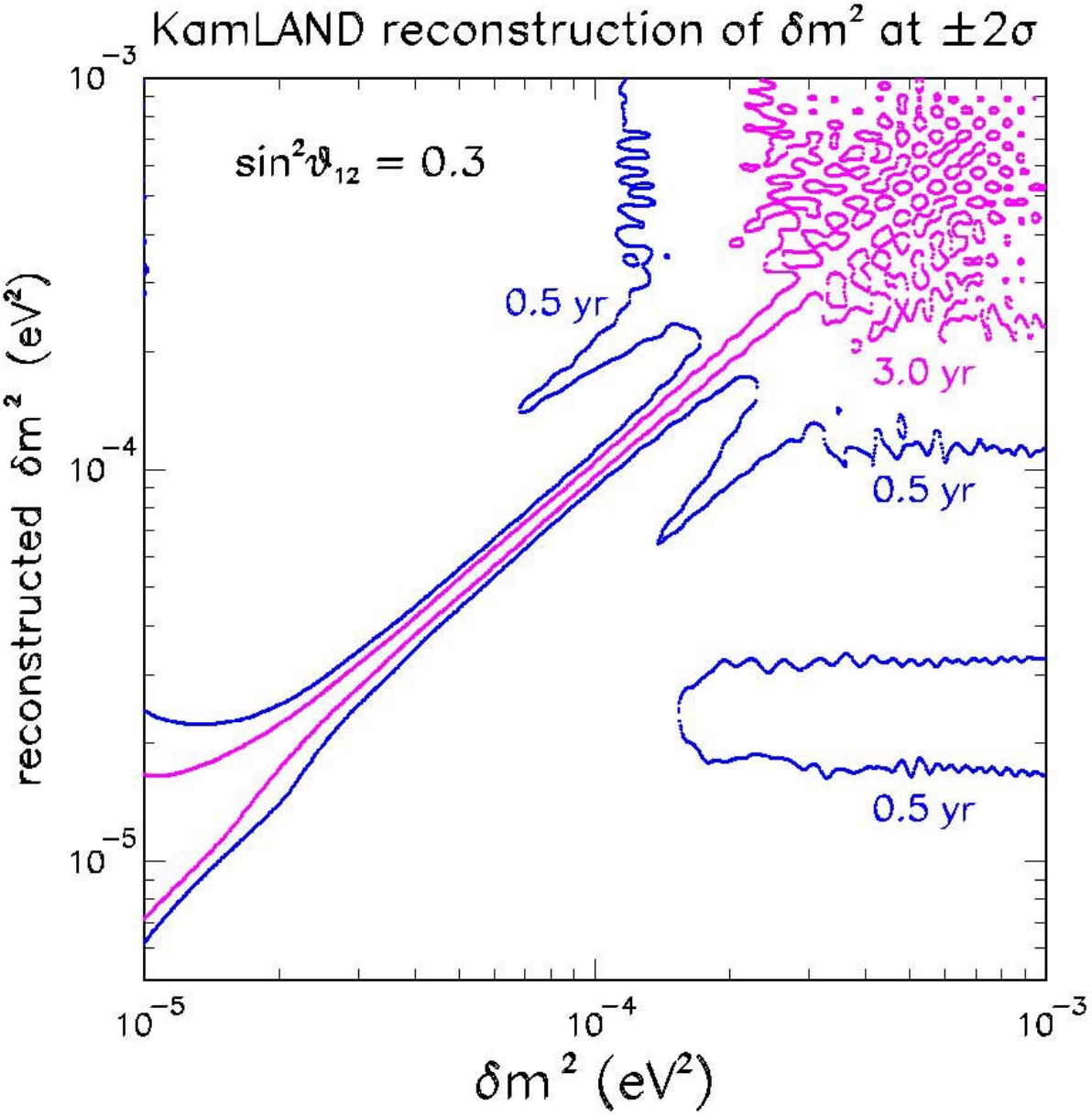

FIG. 6: Simulation of KamLAND results. Reconstructed range of δm^2 at $\pm 2\sigma$, as a function of the true value of δm^2 in abscissa. The true value of $\sin^2\theta_{12}$ is fixed at 0.3. The curves refer to detector exposures of 0.5 and 3 years.

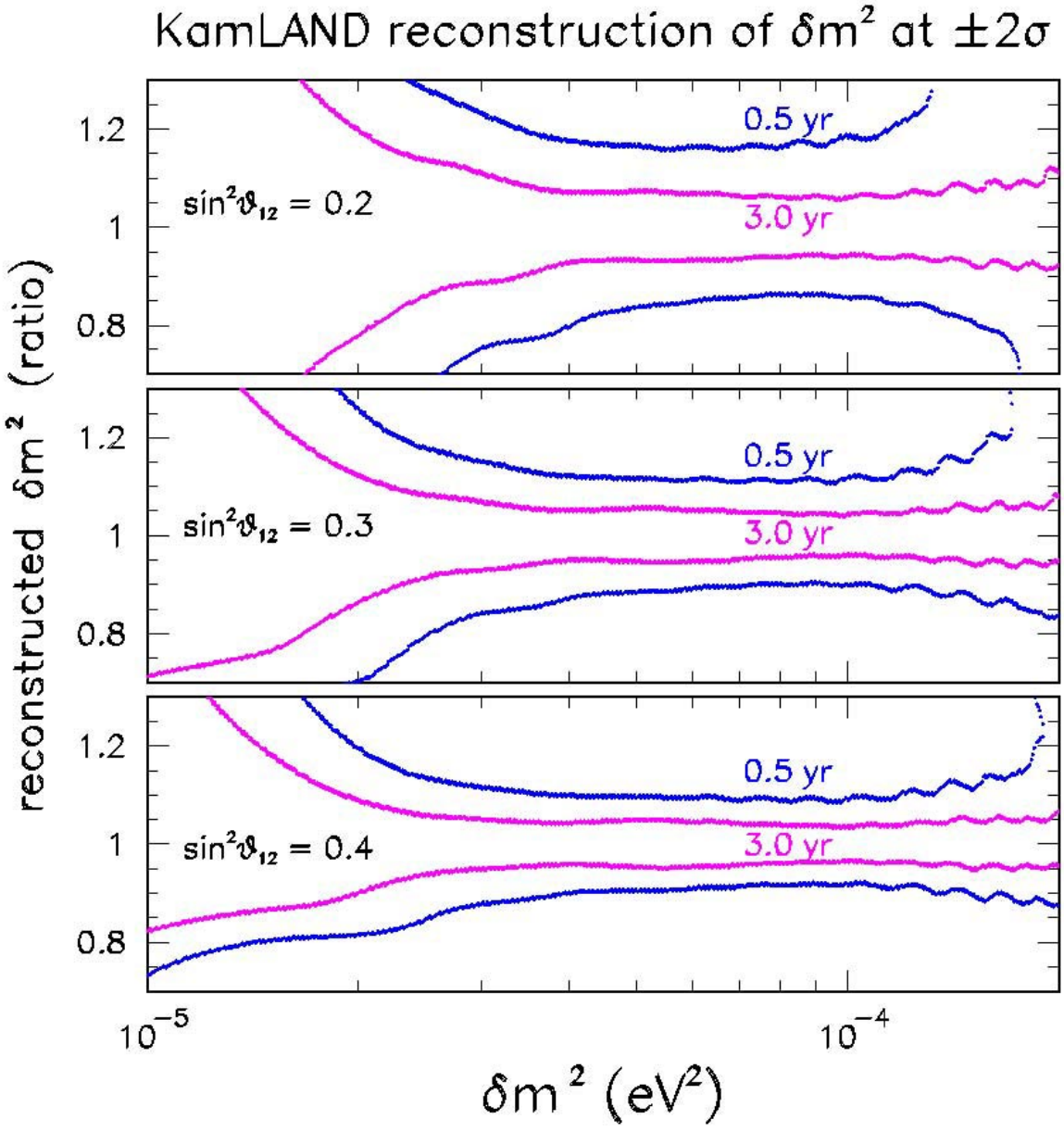

FIG. 7: Simulation of KamLAND results. Reconstructed range of δm^2 at $\pm 2\sigma$ (normalized to the true value of δm^2 in abscissa), for three representative values of $\sin^2\theta_{12}$, and for exposures of 0.5 and 3 years.

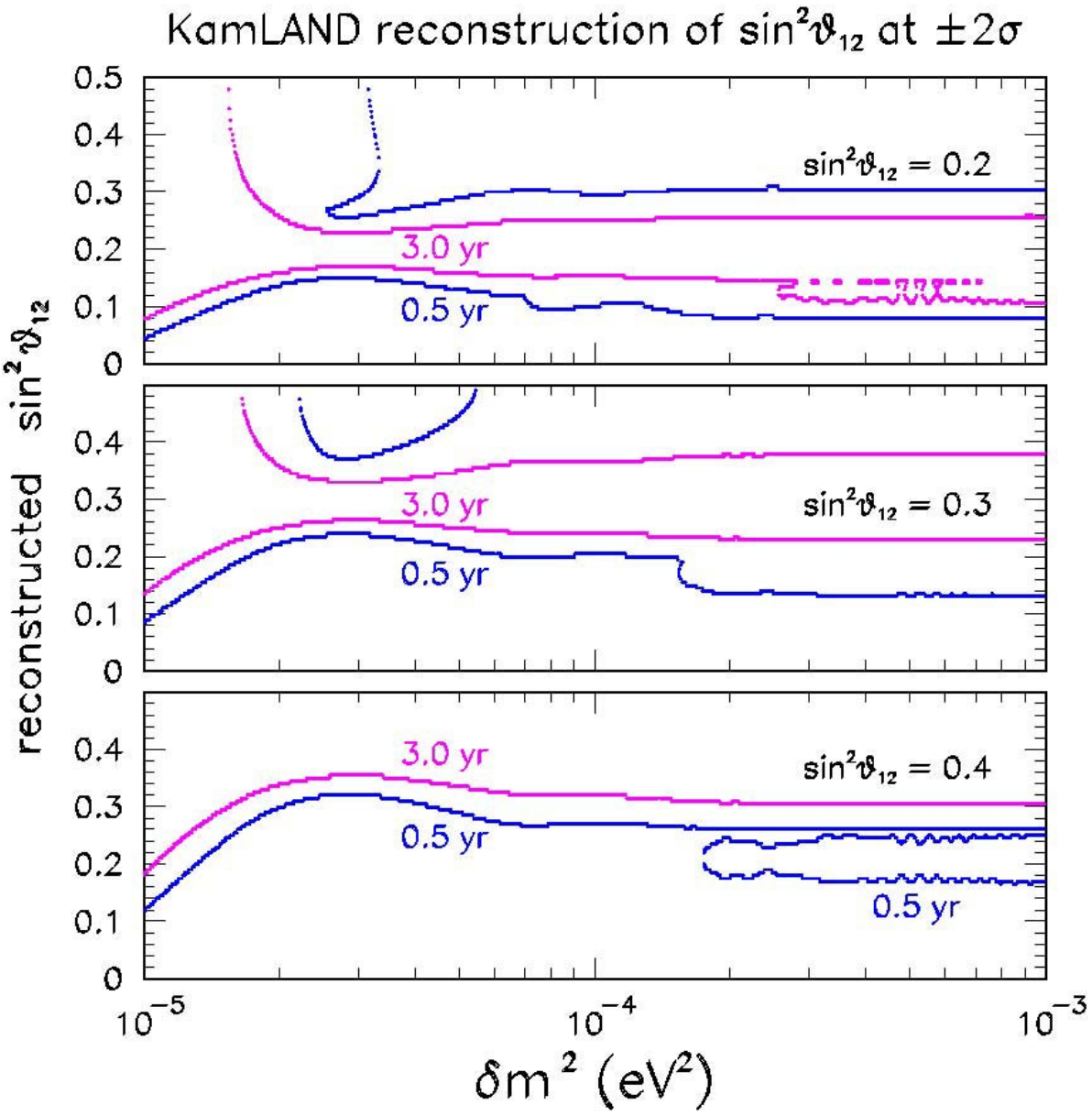

FIG. 8: Simulation of KamLAND results. Reconstructed range of $\sin^2\theta_{12}$ at $\pm 2\sigma$ as a function of δm^2, for three representative (true) values of $\sin^2\theta_{12}$, and for exposures of 0.5 and 3 years.